MAX-PLANCK-INSTITUT FÜR PLASMAPHYSIK

GARCHING BEI MÜNCHEN

Nonlinear instability mechanism in 3-D collisional driftwave turbulence

Dieter Biskamp and Andreas Zeiler

IPP 6/322 August 1994

Die nachstehende Arbeit wurde im Rahmen des Vertrages zwischen dem Max-Planck-Institut für Plasmaphysik und der Europäischen Atomgemeinschaft über die Zusammenarbeit auf dem Gebiete der Plasmaphysik durchgeführt.

Nonlinear instability mechanism in 3-D collisional drift-wave turbulence

D. Biskamp and A. Zeiler
Max-Planck-Institut für Plasmaphysik
D-85748 Garching, Germany

Abstract

Numerical simulations of 3-D collisional drift-wave turbulence reveal a behavior basically different from that found in previous 2-D studies. The linear instability saturates due to energy transfer to small k_z leading to formation of convective cells. The turbulence is sustained by nonlinear transfer processes between $k_z = 0$ and $k_z \neq 0$ modes, the latter acting as a catalyst. The system tends to relax to a nonturbulent poloidal shear flow. Introducing a damping of this flow gives rise to an intermittent behavior, where laminar periods of zero flux alternate with bursts of turbulence and large flux, the transitions occuring on time scale short compared with the linear growth times.

It is now rather generally believed that the cross-field heat and particle transport observed in magnetically confined plasmas is caused by primarily electrostatic small-scale density and potential fluctuations associated with drift-waves, which are energized by the mean density and temperature gradients and excited by collisions or kinetic effects. While in the hot core of a toroidal plasma column fluctuation amplitudes are small $\delta n/n < 10^{-2}$, they become much higher in the cooler edge region $\delta n/n \sim$ 0.1-0.3. The transport effects in the edge plasma play an important role for the global confinement properties. This has become particularly clear by the discovery of the H-mode, a plasma state of significantly improved (high) confinement. The H-mode appears to be intimately connected with a drastic reduction of the density fluctuation level in the edge region. Several theoretical concepts of this transition (and the transition back to the L-mode, the normal (low) confinement state) have been presented. In the presently most widely accepted one the turbulence is stabilized by a strong poloidal shear flow which itself is generated by the turbulence.

Since the plasma in the edge region is collision dominated, drift-wave turbulence in this region can be described in the framework of two-fluid theory. In the simplest model one neglects toroidal (i.e. ballooning) effects, restricts consideration to a slab of narrow radial extent about a resonant surface such that magnetic shear can be omitted, and neglects ion temperature effects. The two-fluid equations essentially reduce to the set of equations for the electric potential φ and the density n introduced by Hasegawa and Wakatani[1].

These are the ion equation of motion

$$\frac{n_0}{\Omega_i}\,\frac{c}{B_0}\,(\partial_t\omega + \mathbf{v}\cdot\nabla\omega) = \frac{1}{e}\nabla_{||}j_{||} + D^{\omega} \tag{1}$$

and the electron continuity equation

$$\partial_t n - n_0'\frac{c}{B_0}\partial_y\varphi + \mathbf{v}\cdot\nabla n = \frac{1}{e}\nabla_{||}j_{||} + D^{n}\ , \tag{2}$$

where $\mathbf{v} = (c/B_0)\hat{\mathbf{z}}\times\nabla\varphi$, $\omega = \nabla_\perp^2\varphi$, and $n_0' = -n_0/L_n < 0$ is the mean density gradient in the negative x-direction. The parallel current $j_{||}$ is obtained from Ohm's law

$$j_{||} = \frac{1}{\eta}\left(\frac{1}{en}\nabla_{||}p_e - \nabla_{||}\varphi\right)\ , \tag{3}$$

where $\eta = \nu_{ei}/\omega_{pe}^2$ is the resistivity. Introducing the standard drift-wave normalizations $\varphi \to (e\varphi/T_e)(L_n/\rho_s)$, $n \to (n/n_0)(L_n/\rho_s)$, $t \to tc_s/L_n$, $\nabla_\perp \to \rho_s\nabla_\perp$, $\nabla_{||} \to L_{||}\nabla_{||}$, with $L_{||}$ a typical parallel wavelength or correlation length, eqs (1), (2) become

$$\partial_t\omega + \mathbf{v}\cdot\nabla\omega = \nabla_{||}^2(n-\varphi) + D^{\omega} \tag{4}$$

$$\partial_t n + \partial_y\varphi + \mathbf{v}\cdot\nabla n = \nabla_{||}^2(n-\varphi) + D^{n}\ . \tag{5}$$

Here the coefficients in the parallel diffusion terms on the r.h.s.'s have been chosen unity, which defines the parallel scale length $L_{||}$,

$$L_{||} = (L_n T_e/m_e c_s \nu_{ei})^{1/2}\ .$$

D^{ω} and D^{n} represent perpendicular viscous dissipation effects, which in the present context should only guaranty regularity of φ, n. Since we want to localize these effects at the smallest scales, D^{ω}, D^{n} are - rather arbitrarily -

chosen as $D^\omega = \mu\nabla_\perp^{(6)}\omega$, $D^n = \nu\nabla_\perp^{(6)}n$, with $\mu = \nu$.

The nonlinear terms $\mathbf{v}\cdot\nabla\omega$ and $\mathbf{v}\cdot\nabla n$ conserve the kinetic energy $E^K = \int v^2 dV$ and the energy of the density fluctuations $E^N = \int n^2 dV$, respectively. Switching on the remaining terms the following quadratic forms of n and φ behave in a particularly simple way, the total energy $E = \frac{1}{2}\int(v^2+n^2)dV$ and the generalized enstrophy $W = \frac{1}{2}\int(n-\omega)^2 dV$, which follow the equations

$$\frac{dE}{dt} = \Gamma - \int\left(\nabla_{||}(n-\varphi)\right)^2 dV - \mu\int\left[(\nabla_\perp^2\omega)^2 + (\nabla_\perp\nabla_\perp^2 n)^2\right] dV \ , \quad (6)$$

$$\frac{dW}{dt} = \Gamma - \mu\int\left[\nabla_\perp\nabla_\perp^2(n-\omega)\right]^2 dV \ , \quad (7)$$

where $\Gamma = \int n v_x dV = -\int n\partial_y\varphi dV$ is the average turbulent plasma flux. Only the Γ terms may be positive and hence drive the turbulence by extracting energy from the (fixed) mean density gradient.

Studies of the Hasegawa-Wakatani (HW) equations (4), (5) have previously been restricted mainly to two-dimensional geometry[2),3)] by assuming $\nabla_{||}^2 \to -k_{||}^2 = -k_z^2$ to be a constant, proportional to the so-called adiabaticity parameter C (large values of C enforce a nearly adiabatic behavior of the density, $n \simeq \phi$, whence the name). For sufficiently weak viscous dissipation the last term in eq. (6) is negligible, such that Γ and parallel dissipation balance each other in stationary turbulence, while the viscous term in eq. (7) remains finite. The spectral properties of quasi-stationary 2-D HW turbulence have recently been studied in detail in the range $0.1 \le C \le 5$[3),4)]. In all cases one finds a maximum of the angle integrated energy spectrum $E_k = \int E_{\mathbf{k}} d\Omega_{\mathbf{k}}$ at $k = k_0$, where $k_0 \simeq 1$ for $C \sim 1$, and k_0 decreases for both decreasing C ($k_0 \simeq k_m$, the mode of maximum linear growth rate) and for increasing C (where $k_0 < k_m$, k_0 decoupling from the linear instability properties). Hence

in 2-D the HW system does not exhibit an inverse cascade and condensation at small k, contrary to the behavior of the Hasegawa-Mima equation[5], to which the HW equations reduce in the limit $C \to \infty$, i.e. $n \to \varphi$. It is hence interesting to investigate the 3-D HW system, where the magnitude of C, i.e. the k_z-spectrum, is established self-consistently. It will be seen, that the 3-D behavior is basically different from that of a 2-D finite-C system, the nonlinear energy transfer in k_z playing a dominant role.

Several studies of 3-D collisional drift-wave models have previously been performed. In Ref. 6 the HW equations were solved in a cylindrical plasma including magnetic shear and curvature, showing the generation of a poloidal shear flow. In Ref. 7 3-D simulations of drift-resistive ballooning modes have been presented. The model includes, besides magnetic shear, toroidal curvature, which gives rise to a ballooning structure of the fluctuations. As in Ref. 6 a poloidal shear flow is generated by the turbulence, which leads to a strong reduction of the turbulence level and the radial transport. In the present work it is shown that the basic features associated with the generation and back-reaction of the shear flow are already described by the simple straight slab model ignoring magnetic shear and curvature. In this model $k_z = k_{||} = 0$ modes (interchange modes or convective cells) are linearly stable. The linear stability properties are, however, dominated by the nonlinear transfer processes. In addition we find that including a damping of the shear flow representing the effect of magnetic pumping, an intermittent behavior of strong turbulence alternating with a quasi-laminar flow is obtained with abrupt transitions.

The 3-D HW equations are solved in a rectangular box of size $2\pi L_x \times 2\pi L_y \times$

$2\pi L_z$ with periodic boundary conditions using a pseudo-spectral method with dealiasing according to the 2/3-rule. The number of modes (or collocation points) are $N_x = N_y = 96$, $N_z = 48$, and the hyperviscosity $\mu = 10^{-4}$, which is small enough to concentrate dissipation at high k in the energy and enstrophy spectra and still prevent spectral accumulation at high k. Modes are linearly unstable for finite $k_z \neq 0$ and sufficiently small $k_\perp$ and stable at large $k_\perp$ due to viscous damping. For the parameters given above the maximum growth rate $\gamma_{max} = 0.15$ is found at $k_x = 0$, $k_y \simeq 1$, $k_z \simeq 0.5$. (For details of the linear stability properties see e.g. Ref. 2.) In these 3-D computations spatial resolution is necessarily smaller than in previous 2-D runs[3),4)], where up to 1024^2 modes have been used. Therefore the focus is not on small-scale spectral properties but on the dynamics of the dominant large-scale eddies. In our standard case the dimensions of the computed system are $L_x = L_y = 6$, which is large enough to allow formation of structures $\gg \rho_s$ ($k_{\perp min}\rho_s = 0.16$), but still small enough to justify neglecting magnetic shear. The parallel dimensions $L_z = 6$ are chosen such as to locate the most unstable mode in the lower half ($n_z = 3$) of the k_z-spectrum. The time step Δt is determined by the requirement that the energy balance (6) be satisfied with sufficient accuracy. A typical run is illustrated in Fig. 1. The initial state is given by a low level of random noise of $\varphi_{\mathbf{k}}$ and $n_{\mathbf{k}}$. Because of the linear instability the fluctuation energy grows exponentially up to time $t \simeq 70$, when nonlinear effects lead to a bend-over. We can identify the nonlinear (quasi-) saturation mechanism by considering the energy spectrum $E(k_z) = \sum_{\mathbf{k}_\perp} E_{\mathbf{k}}$, Fig. 2. During the linear instability the spectrum $E(k_z)$ reflects the linear growth rate with a maximum at $k_z \sim 0.5$, but for $t > 70$

the maximum of $E(k_z)$ is shifted to smaller k_z. Hence the bend-over is due to a nonlinear transfer in k_z from the linearly most strongly driven modes to weakly driven ones leading to the formation of convective cells. The properties in the nonlinear phase are illustrated by the transfer rates of kinetic and density fluctuation energies,

$$T^K(k_z) = Re\left\{\sum_{\mathbf{k}_\perp,\mathbf{k}'} \hat{\mathbf{z}}\cdot(\mathbf{k}\times\mathbf{k}')k'^2\varphi_{\mathbf{k}'}\varphi_{\mathbf{k}-\mathbf{k}'}\varphi_{-\mathbf{k}}\right\}, \tag{8}$$

$$T^N(k_z) = Re\left\{\sum_{\mathbf{k}_\perp,\mathbf{k}'} \hat{\mathbf{z}}\cdot(\mathbf{k}\times\mathbf{k}')n_{\mathbf{k}'}\varphi_{\mathbf{k}-\mathbf{k}'}n_{-\mathbf{k}}\right\}, \tag{9}$$

plotted in Fig. 3 for $t = 240$, a typical time in this nonlinear phase. Since $T^N(0) < 0$, there is a strong transfer of E_k^N from $k_z = 0$ to $k_z \neq 0$, where $T^N(k_z)$ is almost uniformly distributed and thus drives a broad spectrum of rather high-k_z modes[1]. On the other hand one finds an inverse transfer of kinetic energy E_k^K from high to small k_z, in particular to $k_z = 0$. Hence we find that in contrast to the linear instability the turbulence energy is primarily generated by the convection of the density at $k_z = 0$. Since there is no linear coupling to the potential at $k_z = 0$, a nonlinear process using $k_z \neq 0$ modes is needed, the latter acting as a kind of catalyst. In this nonlinear process both convective cells $E(k_z = 0)$ and drift-waves $\sum_{k_z\neq 0} E(k_z)$ are growing. The nonlinear process is illustrated in Fig. 4. Large-scale convective cells drive $k_z = 0$ density fluctuations at broad scales $k_\perp$. These excite $k_z \neq 0$ drift-waves, which in turn reinforce the convective cells. (Since the latter

[1]Since we do not include in the present model the effects of parallel flows and parallel viscosity, the k_z-spectrum is rather flat. There is, however, no spectral accumulation at large k_z.

tend to condensate at $k_\perp \sim k_{min}$ there is no point of increasing the number of modes and increasing the system size L, since contrary to the 2-D case the system cascades to the largest possible eddies.) For $k_z \neq 0$ the $k_\perp$-spectrum still follows roughly the behavior of the linear growth rate with a maximum at finite $k_\perp$. It is interesting to note that only for $k_z \gg 1$, $k_\perp \ll 1$ the fluctuations are nearly adiabatic $n_{\mathbf{k}} \simeq \varphi_{\mathbf{k}}$. While for $k_z \ll 1$, $k_\perp \ll 1$ one finds $\varphi_{\mathbf{k}} \gg n_{\mathbf{k}}$, density fluctuations dominate $n_{\mathbf{k}} \gg \varphi_{\mathbf{k}}$ for k_z, $k_\perp \gtrsim 1$.

In the state dominated by large-scale convective cells, which give rise to strong energy fluctuations ($t \simeq$ 240-280), there is the tendency of condensation to the $k_y = 0$ mode corresponding to a poloidal shear flow. The mechanism is related to but somewhat different from that described in Ref. 8. A main feature of this process, which occurs at $t \simeq 280$, is the quenching of the nonlinear instability described above, since the driving force $\Gamma \propto k_y$ in eqs (6), (7) (corresponding to the vertical arrow in Fig. 4) is switched off. The small-scale drift-wave turbulence decays, since dissipation now exceeds the reduced nonlinear transfer rate. The turbulence decay can also be viewed as the effect of eddy distortion by the shear flow acting on all modes with $k_y \neq 0$ independent of k_z. As the result the system relaxes to a quasi-laminar stationary poloidal flow. (It should be noted that because of the nonuniform velocity shear - the essentially sinusoidal flow profile has two points of vanishing shear - the turbulence does not decay to arbitrarily low amplitudes. Assuming a fixed sinusoidal shear flow results in a stationary rather low nonlinear level of drift-waves located at these points.)

In the present model system imbedded in a homogeneous magnetic field the poloidal shear flow is Kelvin-Helmholtz unstable if the aspect ratio of the

computational box L_y/L_x exceeds unity. Hence for $L_y/L_x > 1$ the poloidal shear flow cannot be set up. Instead the system settles into a turbulent shear flow state in x-direction ($k_x = 0$), which is possible because of the periodic boundary conditions used. In this case Γ is not switched off, the nonlinear instability remains active giving rise to continued growth of both convective cells and drift-waves. Since in a tokamak plasma the poloidal shear flow is Kelvin-Helmholtz stabilized by the poloidal magnetic field[9], we concentrate on the case $L_y/L_x \leq 1$, where the poloidal flow is stable.

In a real toroidal plasma column a poloidal flow is damped collisionally due to magnetic pumping[10]. Modelling the effect we introduce at $t = 400$ a damping term $-\alpha\omega_{\mathrm{k}}$ into eq. (1) for modes with either $k_y = 0$ or $k_x = 0$, where α is a phenomenological parameter. Figure 5 illustrates the subsequent evolution for $\alpha = 10^{-2}$. During the period $t \simeq$ 400-440 the shear flow decays, at first exponentially $\sim e^{-2\alpha t}$, then more rapidly due to nonlinear processes, to a low amplitude, which reintroduces the turbulent flux Γ and in its wake the drift-wave turbulence. The dynamic state is similar to that in the first turbulent phase 200-280 and terminates rather abruptly by the regeneration of a poloidal shear flow state, which again suppresses the nonlinear instability and the turbulent flux. The behavior of alternating periods of shear flow and turbulence, appearing in a burst-like manner, continues. The average duration of quasi-laminar shear flow states is roughly proportional to α^{-1}. The spatial distribution of φ and n in the turbulence phase and the shear flow phase is illustrated in Fig. 6. (If only the poloidal shear flow is damped, the system switches rapidly into a turbulent state of dominant radial shear flow, which as mentioned before leads to unlimited growth of all fluctuations.)

In conclusion we have shown that 3-D collisional drift-wave turbulence is basically different from the behavior of a 2-D system with a given adiabaticity parameter C. The turbulence is not driven by the linear instability mechanism, but by a nonlinear process where large-scale convective cells excite $k_z = 0$ density fluctuations. From these energy is transferred to a broad spectrum of $k_z \neq 0$ drift-waves, where energy is partly dissipated partly transferred back to the convective cells. There is an inherent tendency to generate a shear flow, either in poloidal direction ($k_y = 0$), or, if this flow is Kelvin-Helmholtz unstable, in radial direction ($k_x = 0$). While in the case of a poloidal shear flow the turbulent flux Γ, is switched off, leading to rapid turbulence decay, the fluctuation level is growing without saturation in the case of a radial shear flow. Introducing an explicit damping of the shear flow, representing the effect of magnetic pumping in a toroidal plasma column, generates an intermittent turbulent state, where laminar periods of almost zero flux alternate with turbulent periods of large flux. The transitions occur very rapidly on time scales short compared with the linear growth times. This behavior may be related to the dithering H-mode[11] and the grassy ELM's[12] observed in tokamak plasmas.

Acknowledgments: The authors are grateful to Dr.J.Drake for several useful discussions.

References

[1] A. Hasegawa and M. Wakatani, Phys. Rev. Lett. **50**, 682 (1983)
M. Wakatani and A. Hasegawa, Phys. Fluids **27**, 611 (1984)

[2] A.E. Koniges, J.A. Crotinger, and P.H. Diamond, Phys. Fluids **B4**, 2785 (1992)

[3] D. Biskamp, S.J. Camargo, and B.D. Scott, Phys. Lett. **A 186**, 239 (1994)

[4] S.J. Camargo, D. Biskamp, and B.D. Scott, submitted to Phys. Plasmas

[5] A. Hasegawa, C.G. Maclennen, and Y. Kodama, Phys. Fluids **22**, 2122 (1979)

[6] A. Hasegawa and M. Wakatani, Phys. Rev. Lett. **59**, 1581 (1987)

[7] P.N. Guzdar, J.F. Drake, D. McCarthy, A.B. Hassan, and C.S. Lin,

[8] J.M. Finn, J.F. Drake, and P.N. Guzdar, Phys. Fluids **B4**, 2758 (1992)

[9] s.e.g. S. Chandrasekhar, Hydrodynamic and Hydromagnetic stability (Dover, New York, 1981); B.D. Scott, P.W. Terry, and P.H. Diamond, Phys. Fluids **31**, 1481 (1988)

[10] see e.g. A.B. Hassan and R.M. Kulsrud, Phys. Fluids **21**, 2271 (1978)

[11] s.e.g. H. Zohm et al., Plasma Phys. Control. Fusion **36**, A129 (1994)

[12] s.e.g. T. Ozeki et al., Nucl. Fusion **30**, 1425 (1990)

Figure Captions

Fig. 1 Time evolution of (a) the total turbulence energy E, (b) the drift-wave energy ($k_z \neq 0$), (c) the turbulent flux Γ.

Fig. 2 k_z energy spectrum in linear instability phase $t = 60$, in the nonlinear phase $t = 100$.

Fig. 3 Density and kinetic energy transfer functions $T^N(k_z)$, $T^K(k_z)$ in the phase of strong turbulence $t = 240$.

Fig. 4 Schematic illustration of the nonlinear instability mechanism.

Fig. 5 Time evolution of E and Γ for the same run as shown in Fig. 1, continued at $t = 400$ with a shear flow damping $\alpha = 10^{-2}$.

Fig. 6 Contours of $\varphi(\mathbf{x})$ and $n(\mathbf{x})$ taken for three different cross sections $x = const$, $y = const$, $z = const$ (z-direction is vertical), illustrating the 3-D spatial distributions (a) turbulence phase, $t = 453$, (b) shear flow phase, $t = 512$.

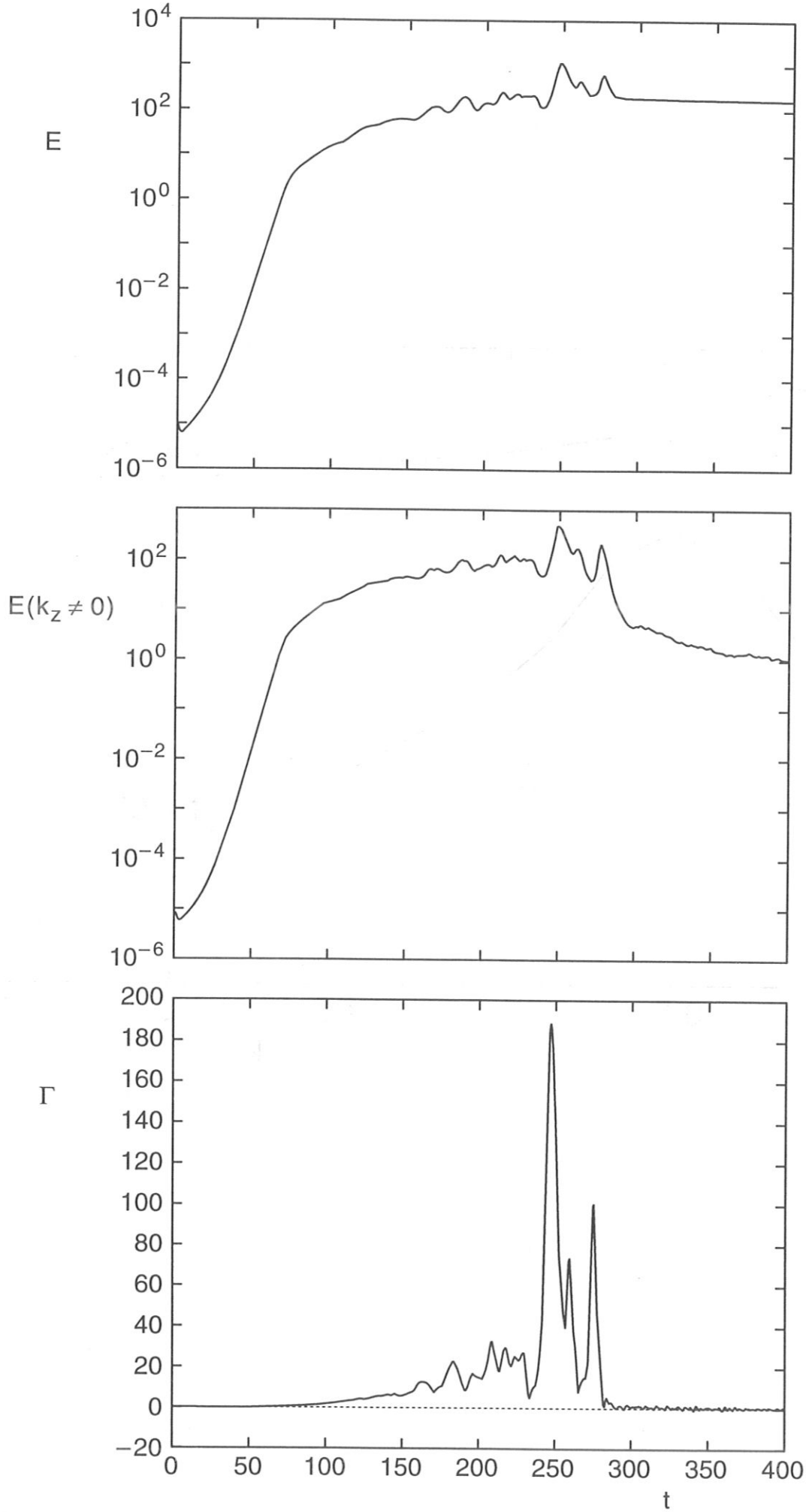
E
10^4
10^2
10^0
10^{-2}
10^{-4}
10^{-6}
$E(k_z \neq 0)$
10^2
10^0
10^{-2}
10^{-4}
10^{-6}
Γ
200
180
160
140
120
100
80
60
40
20
0
−20
0
50
100
150
200
250
300
350
400
t

Fig. 1

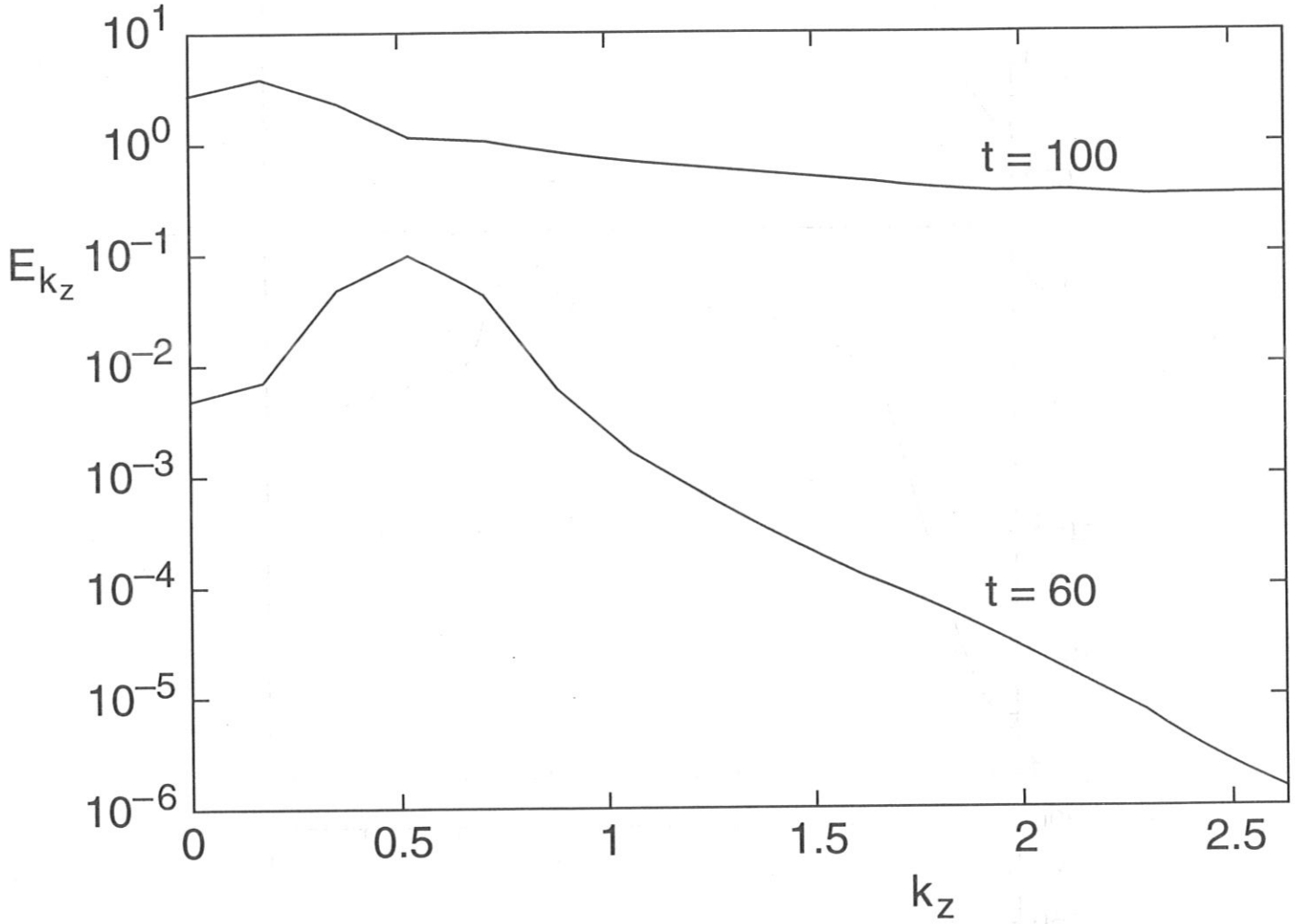

Fig. 2

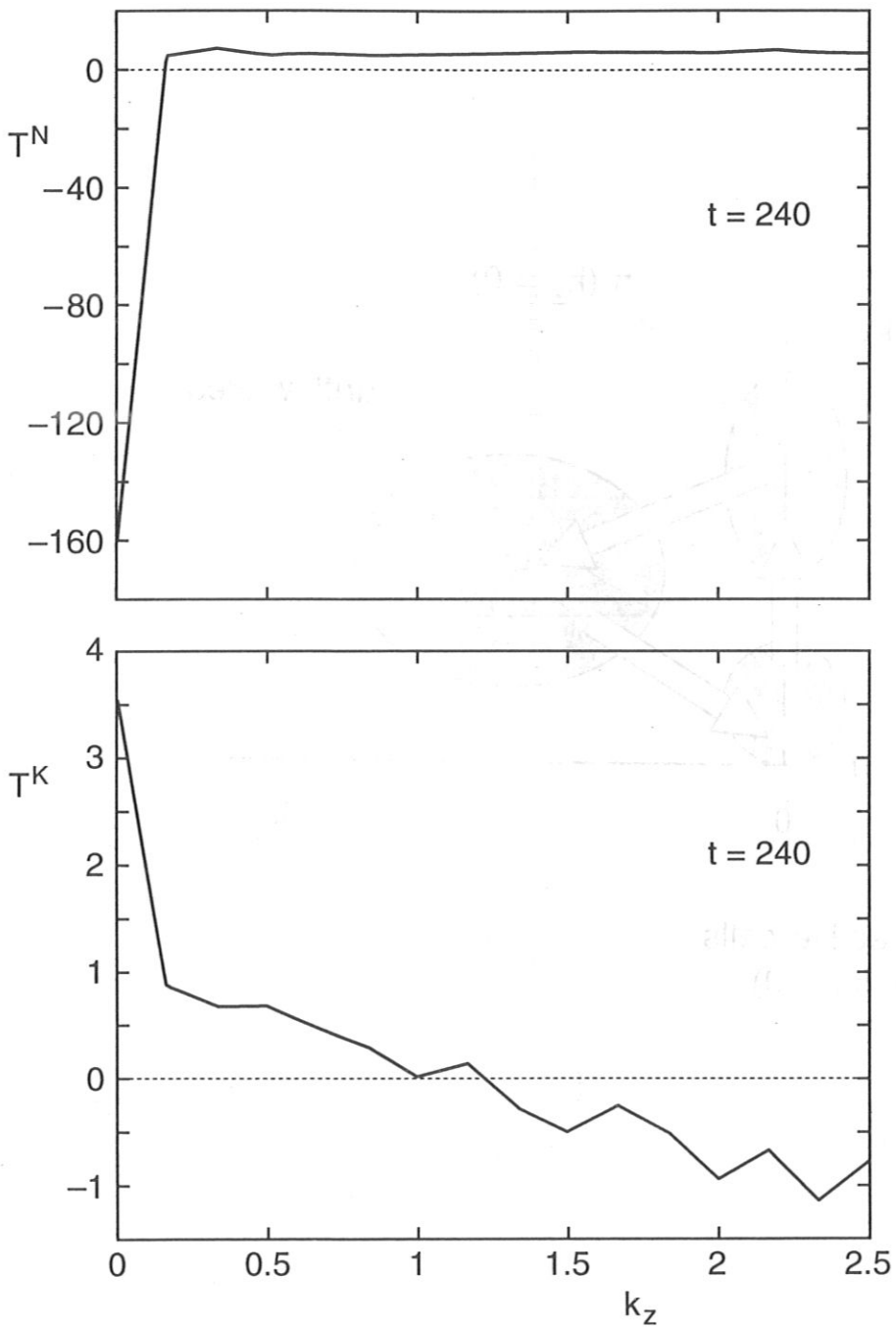

Fig. 3

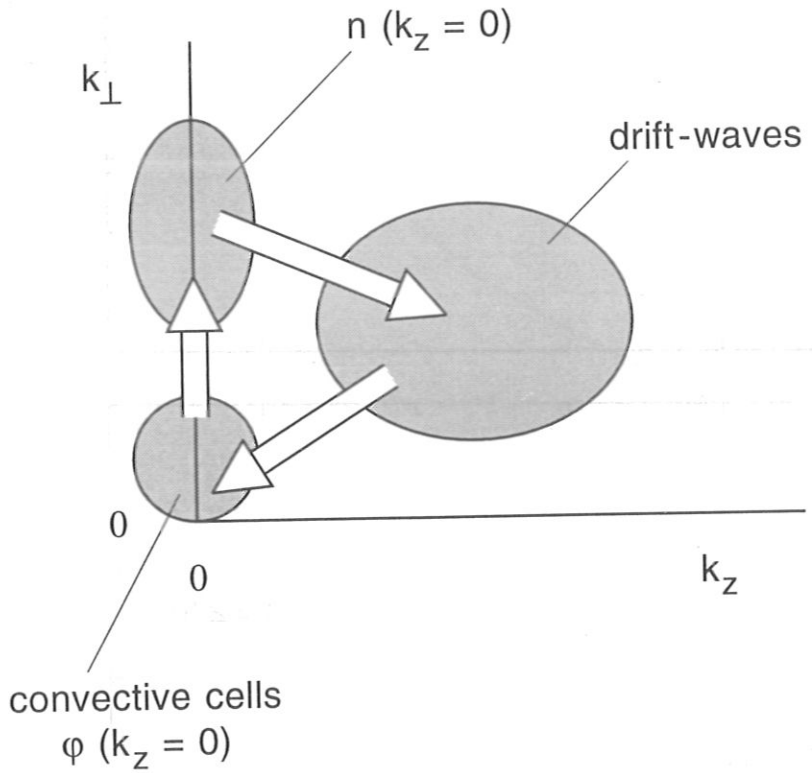

Fig. 4

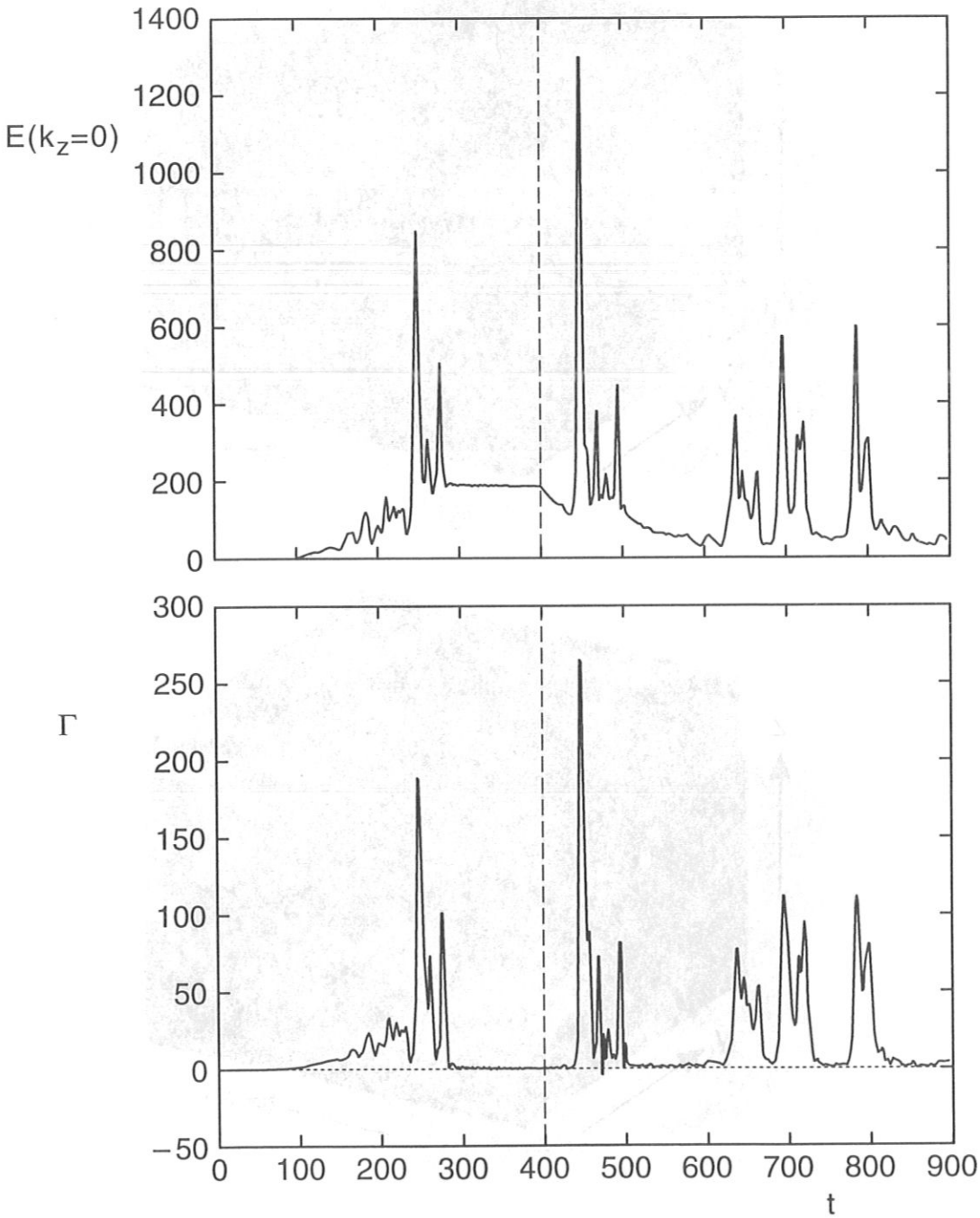
E(k_z=0)
1400
1200
1000
800
600
400
200
0
Γ
300
250
200
150
100
50
0
−50
0
100
200
300
400
500
600
700
800
900
t

Fig. 5

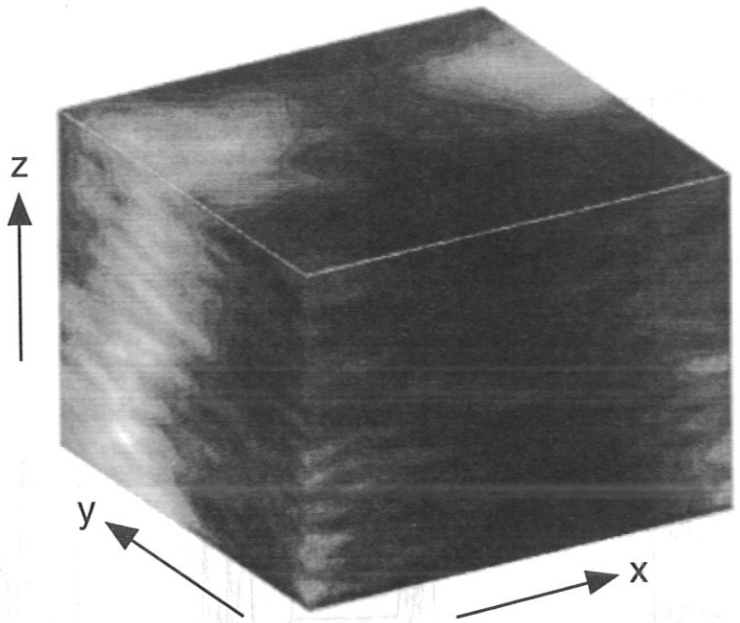

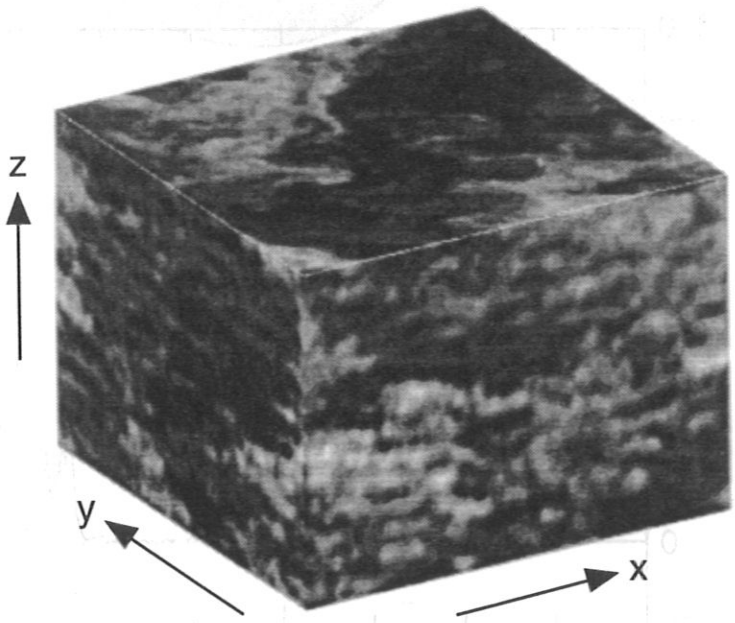

Fig 6a

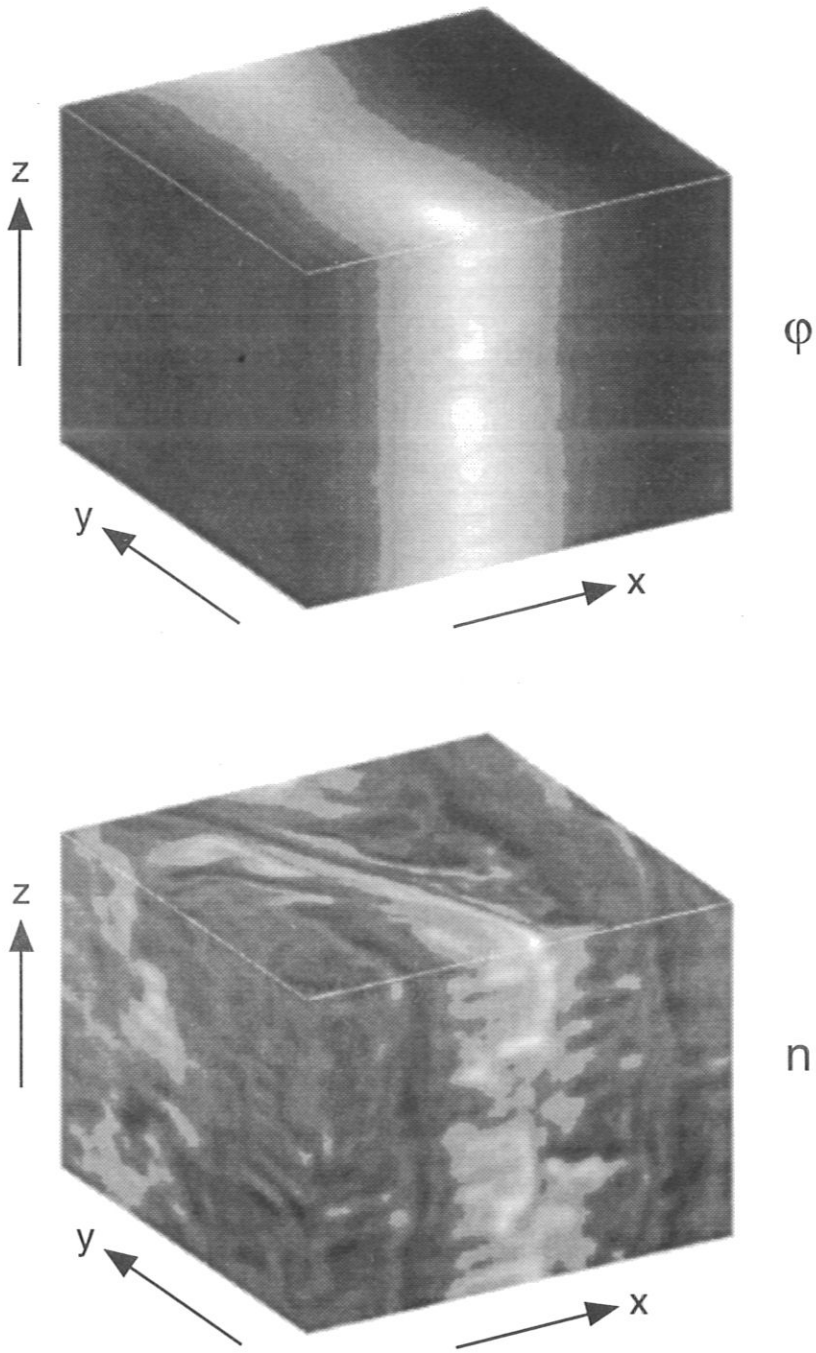

Fig. 66